Elevation of the temperature of liquid films caused by rapid rupturing

Susumu Kono (高野晋),[1,*] Toshihiro Kaneko (金子敏宏),[1,2] and Ichiro Ueno (上野一郎)[1,2]

[1]*Department of Mechanical Engineering, Faculty of Science and Technology, Tokyo University of Science,*
2641 Yamazaki, Noda, Chiba 278-8510, Japan
[2]*Research Institute of Science & Technology, Tokyo University of Science, 2641 Yamazaki, Noda, Chiba 278-8510, Japan*

Although there have been several experimental and numerical works on rapidly rupturing films, measurement of the spatial-temporal temperature during rupturing processes is lacking. Using molecular dynamics simulations, we show that a rupturing film with nanometer thickness generates a non-negligible temperature increase. We demonstrate a correlation between the rupture velocity, the temperature increase, and the initial film thickness. Our findings show that the temperature increase causes changes to the physical properties, which affect the film-rupturing behavior.

The behaviors of films have been of interest for centuries. Dupré [1] and Rayleigh [2] first discussed the dynamics of film rupturing about 100 years ago and the rupture velocity was derived from the conservation of energy in the dominant inertial state. Later, Taylor [3] and Culick [4] improved on that derivation and obtained

$$U = \sqrt{\frac{2\gamma}{\rho e_0}}, \qquad (1)$$

where U is the Taylor-Culick speed, i.e., the characteristic rupture velocity, ρ is the density, γ is the surface tension, and e_0 is the initial film thickness. However, the work done by surface tension on the thin film does not match the kinetic energy based on the velocity from Eq. (1) [5]. A theoretical explanation for this is that the excess kinetic energy is converted to thermal energy [4] due to viscosity dissipation [6]. However, although many experiments [2,7–12] on film rupturing have been performed using high-speed cameras, the variation of the thermal energy has not been directly measured [9,10]. It is quite difficult to observe the predicted temperature increase because the temperature variation is too small to detect with current experimental equipment. Using numerical simulations based on continuum equations, the viscosity contribution to film rupturing and the sheer effect on the surrounding fluid have been elucidated [13–16] and the geometric effect has also been investigated [15]. In addition, the dissipated energy has been confirmed numerically [14], but the heat generation effect has not been discussed. On the nanometer scale, the rupturing behavior is similar to continuum simulations [17]. After rupturing, the liquid deformation to droplets and the resultant dissipated heating have been observed [18], but the expected temperature increase due to this heat generation on rupturing has not been reported. This temperature increase causes the film's properties to vary, which is expected to lead to complicated capillary phenomena. An improved understanding of the relationship between temperature and the physical properties of the film is therefore of considerable interest, as this effect is utilized in industrial applications

such as in diesel engines and ink-jet printers, as well as in atomization and breakup processes.

To evaluate the temperature increase on rupturing, we make the following six assumptions, based on the energy conservation law from the molecular perspective for a microcanonical ensemble. (i) The work done by the surface tension equals the change in the total intermolecular potential [19] such that

$$
\begin{aligned}
2\gamma \Delta A &\approx \Delta E_{\text{pot}} \\
&= E_{\text{pot}}(0) - E_{\text{pot}}(t) \\
&= E_{\text{kin}}(t) - E_{\text{kin}}(0), \qquad (2)
\end{aligned}
$$

where ΔA is the surface difference, ΔE_{pot} is the potential energy difference, E_{pot} and E_{kin} are the potential and kinetic energies of the sums of the liquid molecules, and t is time. Then the potential energy difference is

$$
\begin{aligned}
\Delta E_{\text{pot}} &= \sum \frac{1}{2} m_i \mathbf{v}_i(t)^2 - \sum \frac{1}{2} m_i \mathbf{v}_i(0)^2 \\
&= \sum \frac{1}{2} m_i \mathbf{V}_i(t)^2 + \sum m_i \mathbf{V}_i(t) \cdot \mathbf{v}'_i(t) \\
&\quad + \sum \frac{1}{2} m_i \mathbf{v}'_i(t)^2 - \sum \frac{1}{2} m_i \mathbf{v}'_i(0)^2, \qquad (3)
\end{aligned}
$$

where m_i and $\mathbf{v}_i$ are the masses and velocity vectors of the molecules, respectively; $\mathbf{V}_i$ is the macroscopic velocity vector; and $\mathbf{v}'_i$ is the microscopic velocity, which is often used to define the kinetic temperature in a nonequilibrium system. (ii) The rupture velocity is sufficiently developed to reach the Taylor-Culick speed $\mathbf{V}_i(t) = U$. (iii) The volume over which the energy is dissipated is equal to the volume of the ruptured liquid [1]. (iv) The entire liquid rim (labeled control volume (CV) in Fig. 1) moves at the Taylor-Culick speed. (v) The surface energy lost due to the deformation is equally distributed between the kinetic and dissipated energies [4]. (vi) The temperature of the molecules in the liquid rim is defined using the molecular velocity relative to the Taylor-Culick speed. Then the characteristic temperature increase ΔT_C is derived as

$$\Delta T_C = \frac{2m\gamma}{3k_{\text{B}}\rho} \frac{1}{e_0}, \qquad (4)$$

where k_{B} is Boltzmann's constant. For the rupturing of a film of micrometer-scale thickness, as has been studied in

---

*Corresponding author: j7512701@ed.tus.ac.jp

the past, measuring devices with a 10^{-3} K resolution are required. For a film of nanometer-scale thickness, however, the predicted temperature increase is on the order of 1 K. Here the temperature increase would result in variations of the properties with high-temperature dependences (e.g., surface tension and density). Then the rupturing process would become complicated. Knowledge of the fluid motion, taking the temperature variation into account, is crucial for such tasks as realizing nanotechnology with finer features by creating an isothermal boundary condition and controlling fluids using interfacial phenomena to create a self-assembly system on the nanometer scale.

We therefore attempt to reproduce the rupturing of a thin free liquid film with a nanometer-scale thickness using molecular dynamics (MD). In previous research on ruptured film processes using MD simulations, investigations focused on rupturing velocity [17] and instability with regard to the thickness effect [20] (including dewetting [21,22]); however, disscussion of the temperature increase due to the film rupturing process is lacking. In this paper we report the rupture velocity and the resultant temperature variation as functions of the initial film thickness when the total energy in the system is conserved.

The liquid and vapor molecules interact through a Lennard-Jones potential of the form $\varphi(r) = 4\varepsilon[(\sigma/r)^{12} - (\sigma/r)^6]$, which is truncated for $r < r_c = 3.5\sigma$. Here the parameters used are those for argon: $\sigma = 0.34$ nm and $\varepsilon = 1.67 \times 10^{-21}$ J. Thus, the cutoff distance r_c becomes 1.19 nm here. The target system is numerically modeled as a quasi-two-dimensional periodic box to reduce the simulation cost and obtain long-length rupturing. We use a system with a maximum of 410 247 molecules, contained within the long simulation box, which has length, depth, and height dimensions of 500.00, 5.75, and 40.83 nm, respectively. We conduct the simulations using a microcanonical ensemble. Initially, the precalculation results for a thick liquid film (thickness $e = 20$ nm) under equilibrium conditions at a designated temperature of 85.5 K are analyzed and then, for each thickness we wish to simulate, a liquid film of the desired thickness ($e_0 = 2.1$–6.8 nm) is obtained by taking the simulated molecular information from an appropriately sized section of the presimulated thick film. The designated temperature is set to the median temperature between the melting (83.9 K) and boiling (87.3 K) points of argon under atmospheric pressure. Here the thick liquid film is set to 85.5 K using the velocity-scaling method in the initial stage, which controls the velocities of all molecules and scales them to match the target temperature, and then a microcanonical ensemble simulation is conducted to obtain the equilibrium conditions. Our systems are confirmed as being in the vapor-liquid coexistence phase by a local density distribution analysis at the set temperature. The positions and velocities of the molecules are obtained from the corresponding data for the thick-film molecules; consequently, the liquid film with the target thickness has a flat free surface, the molecule velocities have Gaussian-like distributions, and the molecule positions are consistent with those of real liquids and vapors. Then an initial rupture is placed at the center of the film along the y axis. Note that the width of the initial rupture is sufficiently large to create sustainable rupturing.

Our simulations are conducted using homemade code, which measures the temperature dependence of the density

[20,23,24] and the radial distribution function at 85 K [25] and also confirms the effects of the periodic boundary condition and the curvature of the liquid interface. In the present study, we use the surface tension and viscosity values of the reports cited above to perform a qualitative comparison. The equations of motion are integrated using the velocity Verlet method with a time step of $\Delta t = 5$ fs and the algorithm is validated by monitoring the correlation between the total energy deviation and the time step. It is confirmed that the total energy deviation is proportional to the power of the time step Δt^n, where n is between 3 and 4. The algorithm conserves energy quite well, however, not completely. We checked that the energy drift in the present systems is of the order of -10^{-18} J, which is equivalent to cooling 100 000 molecules to 1 K. Although the temperature decrease cannot be neglected, we can qualitatively discuss the temperature increase, which is approximately 5–10 K. During the initial 100 ps, the velocity-scaling method is applied to the fluid molecules to prevent the cooling due to evaporation [18] of the liquid molecules near the interface, so the density distribution through the liquid-vapor interface is smooth. After 100 ps, a microcanonical ensemble is employed.

A typical simulation result for a rupturing film with an initial liquid-film thickness of $e_0 = 4.1$ nm, which corresponds to 12σ, is shown in Fig. 1. Initially, the surface tension of the liquid-film edge causes a rim to form. Then the edge moves in the x direction while accumulating liquid, causing the rim to grow [8–10,13–17] and some molecules to evaporate from the neck. The number of evaporating molecules is quite small in comparison with the number of initial liquid molecules and can therefore be neglected. Over the range of parameters considered, no capillary waves [13–16,26,27] were observed to emerge from the film in the x direction.

Compared with the results of previous simulations [13–16] with regard to the surface deformation near the rim, our results are quite similar to an inertial state [13] or a state with a moderate Ohnesorge number (Oh) [14–16]. In this work Oh [$=\mu/(2e_0\rho\gamma)^{1/2}$] is also moderate despite the very low viscosity, because the length scale of the rupturing process is also very small, as determined by the characteristic length e_0 (e.g., Oh is approximately 0.6–1.1, which has a viscosity of
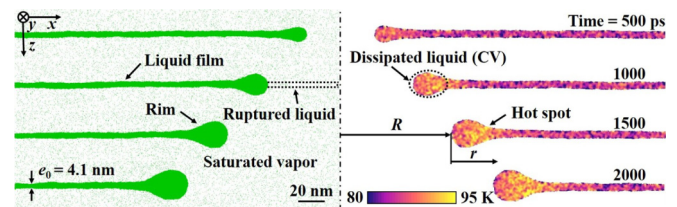
FIG. 1. (Color online) Typical example of rupturing film (side view), with an initial liquid-film thickness and temperature of 4.1 nm and 85.5 K, respectively. The left-hand side depicts the molecules of the rupturing film and the ambient vapor and the right-hand side shows the temperature distribution of the rupturing film only. The region bounded by the dashed lines on the left-hand (right-hand) side represents the ruptured (dissipated (labeled control volume (CV))) liquid. These regions are considered in the discussion of temperature increase estimation in the rupturing film [see assumptions (iii) and (iv) above]. The patchy pattern in the liquid film on the right-hand side represents the thermal fluctuations.

$\mu = 0.3$ mPa s [28] and a surface tension of $\gamma = 13$ mJ/m^2, agreeing with experimental observation [24,29]), and the characteristic time scale of the rupturing process $\tau = \mu e_0 / 2\gamma$ [13] is very small, e.g., 25–75 ps. For each set of conditions, we ran the simulation for over 35τ. Then the rupture velocity was defined as the time average between the velocities for the times between 30τ and 35τ.

Figure 2(a) presents the evaluated velocity as a function of the initial film thickness. The velocity is evaluated by monitoring the rupture area's length as a function of time, as shown in the inset [2,7,8]. The obtained velocity is inversely proportional to the square root of the initial film thickness and the slope and the orders agree with the Taylor-Culick speed, as shown in Eq. (1), for $\rho = 1390$ kg/m^3, calculated in the present simulations, and $\gamma = 13$ mJ/m^2, for liquid argon [24,29].

Previous experiments on rupturing films [2,7–10] have been conducted using a liquid with a surfactant as the test fluid. For the rupturing of a subnanometer-thick film such as a Newton black film, the results are not consistent with the Taylor-Culick speed [8]. This is explained by considering the different characteristics of the pure liquid as the effects of the surfactant elasticity [30] or the surface tension decrease caused by the compression of the surfactant monolayer in the liquid rim [31]. In comparison with previous MD simulations, the retraction shape and the constant rupturing velocity [17,21,22] of the liquid rim are also observed. The liquid films in our simulations are stable both before and after rupturing, apart from the thinnest liquid case ($e_0 = 2.1$ nm). In our system, the short y length prevents instability in the y direction because of the periodic boundary conditions and therefore we must consider one-dimensional instability in the x direction. This unstable film demonstrates other self-induced spontaneous ruptures due to surface instability, referred to as second spontaneous ruptures and triggered by instabilities such as spinodal dewetting [21]. The second spontaneous ruptures in our simulations were observed on the order of 500–1000 ps, conforming to the results of previous simulations [20]. The other cases do not demonstrate second spontaneous ruptures within our simulation time scale and it can therefore be postulated that the instability time constant is larger than the time necessary for the rupturing liquid rim to be approached. As a result of stable conditions or rapid rupturings, therefore, the present study obtains agreement with the order of the Taylor-Culick speed for the rupturing of a pure liquid film with a molecular-scale thickness.

Since the temperature is directly associated with the molecular motion, the macroscopic, spatially averaged temperature at each position is defined using the microscopic local kinetic energy. This local energy is evaluated based on the relative molecular motion with respect to the macroscopic fluid motion, which is defined as the average velocity of the molecules within the cutoff radius r_c at each molecular position.

As can be seen in Fig. 1, the temperature distribution shows a strong x dependence and evolves along with the motion of the rim. We now consider the dependence of the temperature increase on the initial film thickness. Figure 2(b) depicts the characteristic temperature increase observed in films of various initial thicknesses found by monitoring the temperature distribution in the film as a function of time. Figure 2(b) (inset) shows the temporal average of the
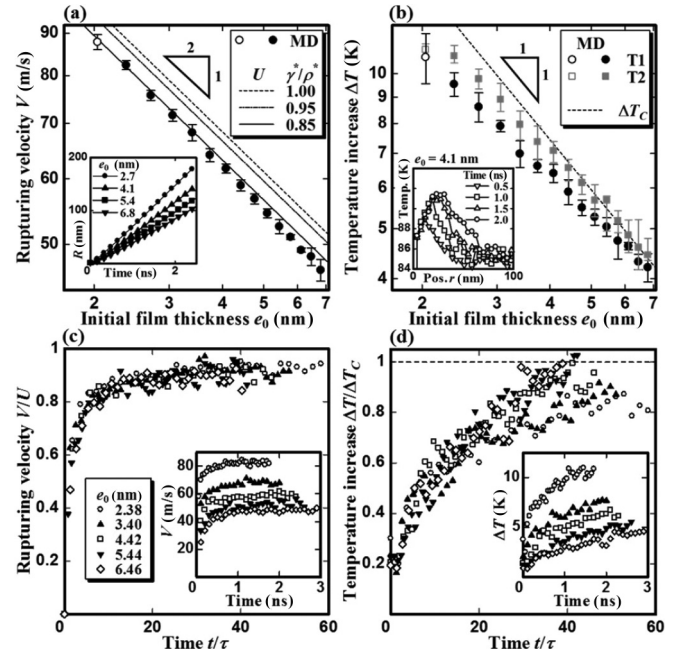
FIG. 2. (a) Dependence of rupture velocity V on initial film thickness e_0. The rupture velocity is calculated from the temporal variation of the rupture length R and results for initial thicknesses of 2.7, 4.1, 5.4, and 6.8 nm are shown in the inset. The temporal development of R is linear during pure rupturing ($t > 100$ ps) after the initial period ($t \leqslant 100$ ps) when the velocity-scaling method is enforced. The rupture velocities are obtained by averaging the velocities for times between 30τ and 35τ. (b) Dependence of temperature increase on initial film thickness. The temperature distributions in the r direction are shown in the inset, which indicates the results under 4.1 nm initial thickness at t ns ($t/\tau[-]$) = 0.5(9.8), 1.0(19.6), 1.5(29.4), and 2.0(39.2). The characteristic temperature increase is defined as the time average of the maximum temperature in the rupturing film (see the inset). Here T1 means the plots are time-averaged values for $30\tau < t < 35\tau$ and T2 represents the time-averaged values from 200 ps before the rim interaction. The plotted points in (a) and (b) represent the average rupture velocities and temperature increases over seven separate simulations and the error bars represent the statistical errors. The closed symbols correspond to conditions without additional rupturing. The open symbols represent a case where a second spontaneous rupture is present in the stationary film. The lines correspond to predictions by Eqs. (1) and (4) for various surface tension to density ratios during rupture [$\gamma^*/\rho^* = (\gamma/\rho)/(\gamma_0/\rho_0) = 1.00, 0.95$, and 0.85] where, for liquid argon in the absence of rupturing, the values are $\rho_0 = 1390$ kg/m^3 and $\gamma_0 = 13$ mJ/m [24,29]. (c) and (d) Typical simulation results for rupturing velocities and temperature increases against time under various initial film thicknesses. Dimensional (inset) and nondimensional values are also given for the time before the rim interaction through the periodic boundary.

temperature distributions at 0.5, 1.0, 1.5, and 2.0 ns, where each average is over the previous 100 ps of the simulation (e.g., the average for 0.5 ns is obtained by averaging over the period from 0.4 to 0.5 ns). The position r indicates the distance from the rim edge to the unperturbed part of the film. It is apparent that a temperature increase exists, located near the rim neck at all times, as shown in Fig. 1. This heat generation process in the film rupturing is considered as being the effect

of the impact between the moving rim and the stationary film, as the location of the temperature increase in our simulations agrees with the position of the most significant momentum difference in the film [15], which causes the most significant temperature increase [4]. The maximum temperature tends to converge over time to the highest value.

The characteristic temperature increase, labeled T1, is defined as the time average of the maximum temperature over the range from $t = 30\tau$ to $t = 35\tau$. This temperature increase is sampled before any rim interaction through the periodic boundary. Therefore, the characteristic temperature increase is considered to be due purely to heat generated by the film rupturing. The order of the characteristic temperature increase, as shown in Fig. 2(b), shows agreement with the order of the earlier discussion on temperature increase estimation in the rupturing film (the estimate is represented by the dashed line), however, there is clear discrepancy between the simulation results and Eq. (4). As shown in Figs. 2(c) and 2(d), the rupturing velocities are almost converging at $t = 30\tau$, but the temperature increases are not. For the thicker cases, e.g., $e_0 = 5.44$ and 6.46 nm, we can see the temperature increase trends have almost converged by approximately $t = 40\tau$. However, the thinner cases, e.g., $e_0 = 2.38, 3.40$, and 4.42 nm require more time for the temperature increase trends to converge. The redefined values of the temperature increases are represented by the T2 trend line in Fig. 2(b). The T2 plots are the time-averaged values between 200 ps, before the rim interaction, which is the limiting condition of our simulation. The difference in the conversion time causes a large discrepancy and, considering the effect of the conversion times, the characteristic temperature increase is in slight agreement with Eq. (4), qualitatively.

The temperature increase due to dissipation is first verified qualitatively, as shown in Fig. 2(b). Considering the observed temperature increase, the surface tension and density ratio $\gamma^*/\rho^* = (\gamma/\rho)/(\gamma_0/\rho_0)$ decrease by about 7%–14%, corresponding to $\Delta T = 5$–10 K under these conditions [24,29]. Modification of the Taylor-Culick speeds by variation of this ratio is shown in Fig. 2(a). These results indicate good agreement with the MD simulation results, but it should be noted that this is a qualitative analysis. Therefore, the heat generation contribution is important for understanding the rapid film rupturing mechanism or nanometer-scale phenomena. This could be a key idea in elucidating unexplained rupturing phenomena [32].

We have performed a series of large MD simulations of film rupturing on the nanometer scale and obtained agreement with the order of the Taylor-Culick speed [3,4]. Additionally, we detected a significant temperature increase during rupturing [4], especially near the rim. This temperature increase agrees with the order of our estimation and the temperature distribution has been determined by direct measurement. Our results suggest that the contribution of the temperature increase produced by the dissipation must be considered when studying many capillary phenomena [33,34] that show rapid surface deformation [30–32,35] such as atomization, jets, foam coarsening, and fragmentation. Therefore, we concluded that the dissipation energy is not negligible on the nanometer scale or in systems with rapid surface deformation.

[1] A. Dupré, Ann. Chim. Phys. **4**, 194 (1867).

[2] L. Rayleigh, Nature(London) **44**, 249 (1891).

[3] G. I. Taylor, Proc. R. Soc. London Ser. A **253**, 313 (1959).

[4] F. E. Culick, J. Appl. Phys. **31**, 1128 (1960).

[5] P.-G. de Gennes, Faraday Discuss. **104**, 1 (1996).

[6] H. Lamb, *Hydrodynamics* (Dover, New York, 1932).

[7] W. E. Ranz, J. Appl. Phys. **30**, 1950 (1959).

[8] W. R. McEntee and K. J. Mysels, J. Phys. Chem. **73**, 3018 (1969).

[9] I. Liebman, J. Corry, and H. E. Perlee, Science **161**, 373 (1968).

[10] A. B. Pandit and J. F. Davidson, J. Fluid Mech. **212**, 11 (1990).

[11] G. Debrégeas, P. Martin, and F. Brochard-Wyart, Phys. Rev. Lett. **75**, 3886 (1995).

[12] G. Debrégeas, P.-G. de Gennes, and F. Brochard-Wyart, Science **279**, 1704 (1998).

[13] M. Brenner and D. Gueyffier, Phys. Fluids **11**, 737 (1999).

[14] G. Sünderhauf, H. Raszillier, and F. Durst, Phys. Fluids **14**, 198 (2002).

[15] N. Savva and J. W. M. Bush, J. Fluid Mech. **616**, 211 (2009).

[16] L. Gordillo, G. Agbaglah, L. Duchemin, and C. Josserand, Phys. Fluids **23**, 122101 (2011).

[17] C. Hwang, J. Hsieh, K. Cuang, and J. Liao, Physica A **256**, 333 (1998).

[18] J. Koplik and J. R. Banavar, Phys. Fluids A **5**, 521 (1993).

[19] J. Israelachivili, *Intermolecular and Surface Forces* (Academic, London, 2011).

[20] J. Weng, S. Park, J. R. Lukes, and C. Tien, J. Chem. Phys. **113**, 14 (2000).

[21] J. Koplik and J. R. Banavar, Phys. Rev. Lett. **84**, 4401 (2000).

[22] E. Bertrand, T. D. Blake, V. Ledauphin, G. Ogonowski, J. De Coninck, D. Fornasiero, and J. Ralston, Langmuir **23**, 3774 (2007).

[23] S. Maruyama, S. Matsumoto, and A. Ogita, Thermal Sci. Eng. **2**(1), 77 (1994).

[24] S. H. Lee, Bull. Korean Chem. Soc. **33**, 167 (2012).

[25] J. L. Yarnell, M. J. Katz, R. G. Wenzel, and S. H. Hoenig, Phys. Rev. A **7**, 2130 (1973).

[26] N. Y. Liang, C. K. Chan, and H. J. Choi, Phys. Rev. E **54**, R3117 (1996).

[27] A. Buguin, L. Vovelle, and F. Brochard-Wyart, Phys. Rev. Lett. **83**, 1183 (1999).

[28] W. T. Ashurst and W. G. Hoover, Phys. Rev. A **11**, 658 (1975).

[29] E. A. Guggenheim, J. Chem. Phys. **13**, 253 (1945).

[30] L. J. Evers, E. J. Nijman, and G. Frens, Colloids Surf. A **149**, 521 (1999).

[31] A. T. Florence and G. Frens, J. Phys. Chem. **76**, 3024 (1972).

[32] H. Lhuissier and E. Villermaux, Phys. Rev. Lett. **103**, 054501 (2009).

[33] P.-G. de Gennes, F. Brochard-Wyart, and D. Quéré, *Capillary and Wetting Phenomena: Drops, Bubbles, Pearls and Waves* (Springer, New York, 2004).

[34] Y. Pomeau and E. Villermaux, Phys. Today **59**(3), 39 (2006).

[35] J. C. Bird, R. de Ruiter, L. Courbin, and H. A. Stone, Nature (London) **465**, 759 (2010).